Anomalous electrical resistivity, bcc phase stability, and superconductivity in titanium-vanadium alloys*

E. W. Collings
Metal Science Group, Battelle, Columbus Laboratories, Columbus, Ohio 43201
(Received 2 November 1973)

Precise measurements of the electrical resistivities ρ of a series of Ti-V alloys have been made in the 77–300-K temperature range. The isothermal composition dependences are shown to be anomalously large (by an amount ρ_{anom}) over a concentration range of from about 12-at.% to at least 70-at.% V. Throughout this range $\rho_{anom,77}$ is larger than $\rho_{anom,300}$. Furthermore, within the composition range of 20–33-at.% V, $(\rho_{77} - \rho_{300})_{anom}$ exceeds the decrease in ideal resistivity between 300 and 77 K, leading to a net negative temperature coefficient of resistivity for those alloys. The results are discussed in the context of transition-metal binary-alloy phase stability, expressed in terms of soft phonons which become more and more localized as the solute concentration increases in the average electron-to-atom ratio range 4.1 to 5.0. A connection is made with superconductivity in alloys formed between groups-IV and -V transition metals. It is pointed out that the phonons of instability, which are responsible for the anomalous resistivity, also favor superconductive coupling and consequently a relatively "high" T_c; but that at the same time, this effect must compete with a proximity-effect-induced lowering of the average T_c by the product of the lattice instability (viz., ω phase), which itself has a very low T_c.

I. INTRODUCTION

As a part of a series of studies[1,2] of the electronic and structural (i.e. physical and metallurgical) properties of Ti-based transition-metal-binary (i.e. Ti-T_2) alloys, electrical resistivity in the Ti-V system was investigated in the temperature range 77–300 K. In an earlier paper, [2] anomalies in both the resistivity temperature dependence ($d\rho/dT$) and resistivity composition dependence ($d\rho/dc$) exhibited by Ti-Mo (7–15 at.%) in the temperature range 4–300 K were attributed to reversible ω-phase precipitation. The appearance of the ω phase is a result of the increasing instability of the bcc transition-metal lattice as the average electron-to-atom ratio $\bar{e}$ decreases towards 4.1. The selection of Ti-V as a system for further anomalous resistivity study is justifiable for several reasons: (a) Whereas Mo, the solute of the previous investigation, is a group-VI ($\bar{e} = 6$) element, V is from group-V ($\bar{e} = 5$). The Ti-V results taken together with those of the earlier work help to throw some light on the importance of average electron-to-atom ratio as a descriptor of electronic and structural properties. (b) The group-V transition elements V, Nb, and Ta, are themselves on the threshold of bcc instability[3]; alloying to their "left" with Ti or Zr enhances this instability, resulting eventually in a martensitic structural transformation to hcp. (c) Ti-V is related to the technically useful superconductors Ti-Nb and Zr-Nb; consequently, experimental information on lattice instability in Ti-V alloys will also have some bearing on the structural and superconducting properties of those alloys.

In all studies of alloys, information regarding the metallurgical states of the samples is of fundamental importance. For Ti-V we were guided by the equilibrium and nonequilibrium phase diagrams of Figs. 1(a) and 1(b), respectively. Figure 1(b) shows that the room-temperature structures of Ti-V alloys quenched from, typically, 1000 °C into iced brine are apparently bcc (β) down to a solute concentration of about 12 at.% ($\bar{e} = 4.12$). The β structure at room temperature is absolutely unstable for $\bar{e} \lesssim 4.1$ and transforms spontaneously to the hcp-based martensitic structure α′. Optical micrographs spanning the critical concentration range are shown in Fig. 2(a). Martensitic structures are clearly present in the 6- and 12-at.% alloys. Ti-V (15 at.%) and Ti-V (25 at.%) appear to be single phase, presumably bcc; but according to the literature[4] quenched Ti-V alloys in the concentration range 13–25 at.% contain ω-phase precipitates. ω phase,[5] in this context, is a submicroscopic precipitate, hexagonal in crystal structure and occurring as a result of the instability of the quenched bcc lattice. As the V concentration increases from 13 at.%, the precipitate size decreases; at the same time, sharp electron-diffraction spots give way to diffuse spots and finally to haloes, which persist in gradually decreasing intensity all the way across to pure V. This situation, in which there is no sharp delimitation of the β+ω field, is represented by the gradual shading in Figure 2(b). Neither is there a sharp line of demarcation between the α′ and β+ω regions. In fact, the results of room-temperature magnetic-susceptibility studies of the Ti-V system (to be described elsewhere) indicate

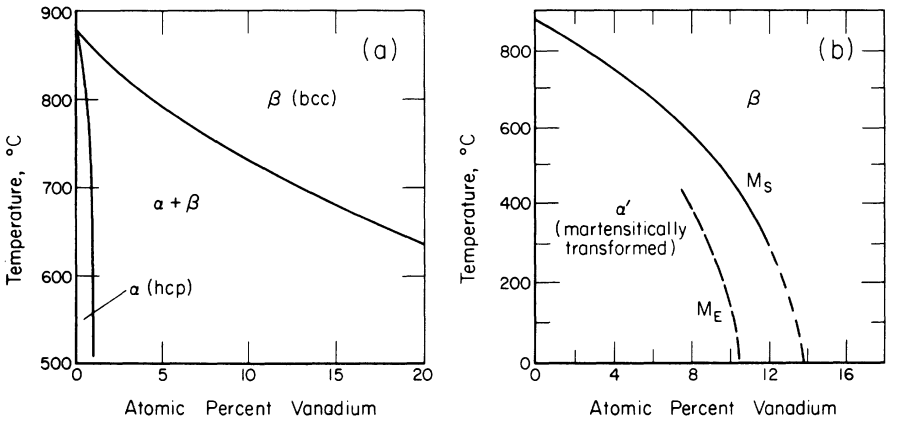

FIG. 1. (a) Ti-V equilibrium phase diagram—after Ref. 6. (b) Ti-V nonequilibrium phase diagram, for alloys quenched from the elevated-temperature single-phase bcc field to the temperatures indicated on the scale—data of P. Duwez [Trans. Am. Soc. Met. 45, 934 (1953)] as modified by the results of metallographic and other studies carried out in this laboratory. M_S indicates the start of the martensitic transformation and M_E the end.

that the α' regime actually terminates with Ti-V (10.5 at.%), while Ti-V (12 at.%) contains a mixture of α' and either ω or $\omega + \beta$ phases.

Electrical-resistivity measurements have occasionally been made during previous metallurgical investigations of the Ti-V system. Where comparisons are possible, the present results are not in conflict with the earlier data. For example, the composition dependence of resistivity measured by Adenstedt *et al.*[6] on a series of bcc Ti-V alloys is in agreement with the appropriate segment of the resistivity isotherm of Fig. 4 (Sec. III B). In addition, the very small negative $d\rho/dT$ (~ -0.14 $\mu\Omega$ cm/K) obtained by Brotzen *et al.*[7] during measurements on quenched Ti-V (19 at.%) is reflected in the temperature-dependence data of Fig. 5 (Sec. III B).

II. EXPERIMENTAL DETAILS

A. Alloy preparation

Fourteen Ti-V alloy ingots were prepared from high-purity ingredients[8] by multiple arc melting on a water-cooled copper hearth. The resulting ingots were cut into pieces suitable for the measurement of various physical properties such as low-temperature specific heat, magnetic suscep-

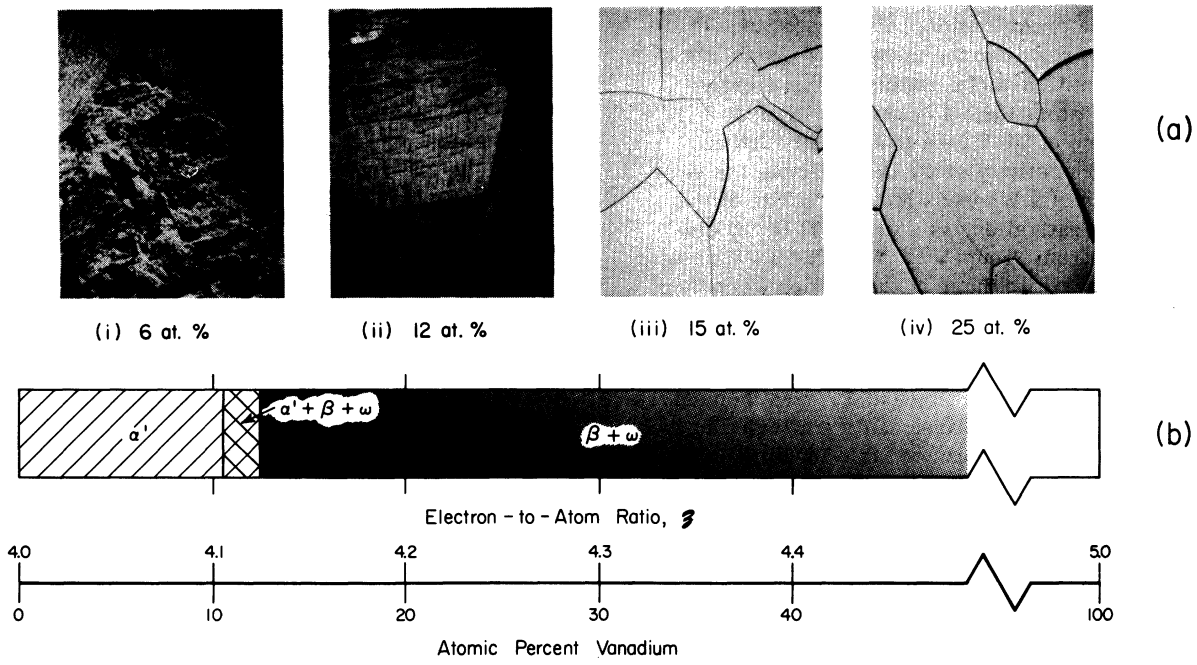

FIG. 2. (a) Optical micrographs (original magnification 50×) of representative quenched Ti-V alloys. (b) Structure observed, or deduced to be present, in 30-g ingots after quenching into iced brine.

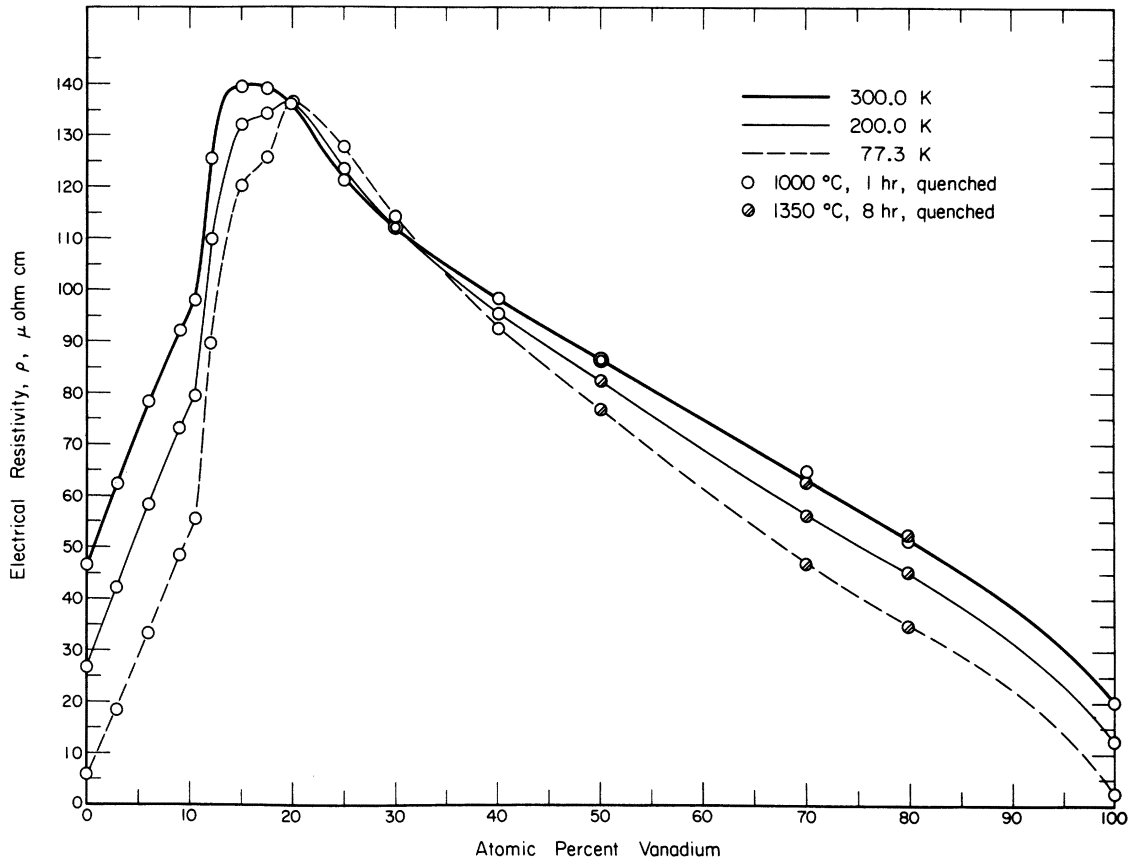

FIG. 3. Resistivity-composition isothermals for Ti-V. The actual liquid-nitrogen-point data are plotted. The 200.0-K data were obtained from measurements at ~200 ± 1 K, corrected using $[d\rho/dT]_{77}^{\sim 200}$; the 300.0-K data were obtained from measurements at ~298 ± 1 K after applying $[d\rho/dT]_{\sim 273}^{\sim 300}$.

tibility, NMR (powder), optical microstructure, and the electrical resistivity considered here. Encapsulated specimens were then annealed in a Ti-gettered argon environment for 1 h at 1000 °C and quenched into iced brine. Coring, which occurred in alloys whose vanadium concentrations were greater than about 50 at.%, was practically eliminated by a second annealing[9] for 8 h at 1350 °C.

TABLE I. Results of the present measurements of electrical resistivity (ρ, $\mu\Omega$ cm) and resistivity-temperature dependence ($d\rho/dT$, $\mu\Omega$ cm K^{-1}) in six samples of unalloyed Ti.

Sample[a]	ρ 300.0 K	ρ 273.2 K	$\left.\frac{d\rho}{dT}\right\|_{273}^{300}$	ρ 200.0 K	ρ 77.3 K	$\left.\frac{d\rho}{dT}\right\|_{77}^{200}$
Ti-1	46.6_1	41.0_1	0.209	26.7_6	5.9_0	0.170
Ti-2	46.6_4	41.0_2	0.209	26.7_6	5.9_9	0.169
Ti-3	46.5_2	40.8_5	0.210	26.7_7	6.0_7	0.169
Ti-4	46.3_5	40.8_0	0.207	26.7_1	6.0_1	0.169
Ti-5	45.3_0	39.8_7	0.203	26.2_3	5.6_7	0.166
Ti-6	47.2_7	41.5_0	0.215	27.2_2	6.5_3	0.166

[a]Samples 1 through 4 were cut from an arc-melted button of TMC (Titanium Metals Corp.) titanium. Sample 5 was turned down from a swaged $\frac{1}{4}$-in.-diameter rod prepared from the same starting material; and sample 6 was turned down from a "crystal bar" of iodide Ti. Samples 5 and 6 are probably less representative of polycrystalline Ti than are samples 1 through 4.

TABLE II. Resistivity (ρ, $\mu\Omega$ cm) and resisitivity-temperature dependence ($d\rho/dT$, $\mu\Omega$ cm K^{-1}) in polycrystalline pure Ti (Samples 1 through 4, Table I) and pure V.[a]

Metal	ρ 300.0 K	ρ 273.2 K	$\left.\frac{d\rho}{dT}\right\|_{273}^{300}$	ρ 200.0 K	ρ 77.3 K	$\left.\frac{d\rho}{dT}\right\|_{77}^{200}$
Ti	46.5_3	40.9_2	0.209	26.7_5	5.9_9	0.169
(Std. dev.)	(0.2_4%)	(0.2_6%)		(0.1_1%)	(1.2%)	
V	20.3	18.3	0.073	12.9	2.4_3	0.085

[a]V data from G. T. Meaden, *Electrical Resistivity of Metals* (Plenum, New York, 1965), Table II, p. 16.

B. Resistivity sample preparation and geometrical considerations

The annealed-and-quenched resistivity specimens, 1 in. or so in length, were ground to a 0.1-in.-square cross section. Errors due to departures from uniform cross-sectional area were greatly reduced by assigning to each specimen an *effective reciprocal area for resistivity*, $A_{eff}^{-1} = (1/n)\sum_1^n A_i^{-1}$, $n = 5$. The accuracy of the measured

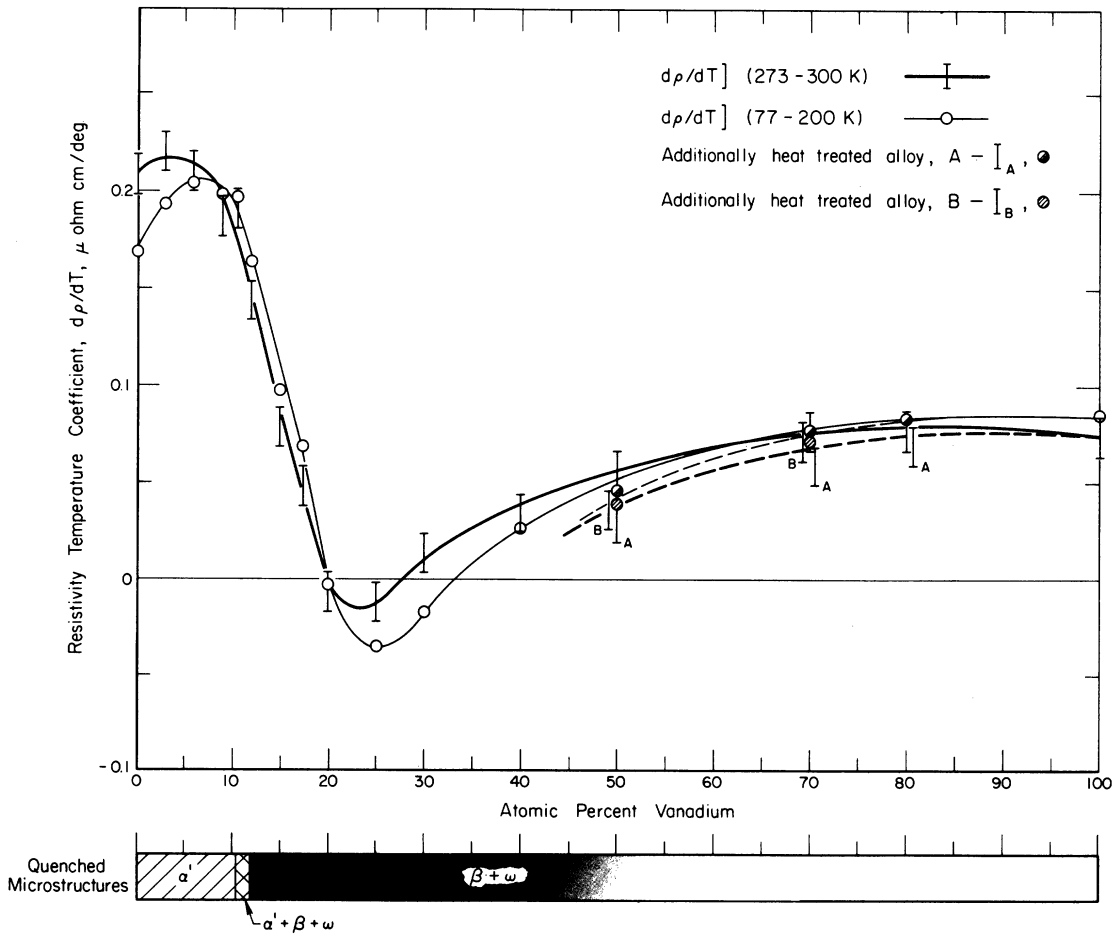

FIG. 4. Resistivity-temperature coefficients in two temperature ranges (273–300 K and 77–200 K) for Ti-V alloys. Additional heat treatment produced slight changes in the submicrostructures, resulting in small changes in resistivity-temperature dependences as indicated by the chain lines.

TABLE III. Results of the present measurements of electrical resistivity (ρ, $\mu\Omega$ cm) and resistivity-temperature dependence ($d\rho/dT$, $\mu\Omega$ cm K^{-1}) on annealed and quenched Ti-V alloys.[a]

Nominal vanadium concentration (at.%)	ρ 300.0 K	ρ 273.2 K	$\left.\frac{d\rho}{dT}\right\|_{273}^{300}$	ρ 200.0 K	ρ 77.3 K	$\left.\frac{d\rho}{dT}\right\|_{77}^{200}$
0	46.5_3	40.9_2	0.209	26.7_5	5.9_9	0.169
3	62.4_0	56.5_0	0.220	42.1_9	18.5_3	0.193
6	78.1_5	72.5_2	0.210	58.1_8	33.3_2	0.203
9	92.1_2	87.1_1	0.187	73.1_2	48.7_0	0.199
10.5	97.9_9	92.9_0	0.190	79.5_0	55.5_0	0.196
12	125.4_5	121.6_0	0.143	109.8_2	89.6_7	0.164
15	139.6_2	137.5_2	0.078	132.0_1	120.0_7	0.097
17.5	139.0_4	137.7_7	0.048	134.2_2	125.7_8	0.069
20	136.7_8	136.9_6	−0.007	136.3_0	136.8_4	−0.004
25	121.1_3	121.4_7	−0.012	123.2_8	127.6_4	−0.035
30	112.0_8	111.7_2	0.014	112.0_0	114.1_1	−0.017
40	98.3_7	97.4_6	0.034	95.5_1	92.3_7	0.026
50	86.3_0	84.9_5	0.057	...	...	...
50[b]	86.8_3	86.0_5	0.029	82.2_3	76.7_1	0.045
50[c]	92.0_3	91.0_4	0.037	87.6_1	82.8_1	0.039
70	65.0_3	63.0_0	0.076	...	...	...
70[b]	62.8_7	61.2_8	0.059	56.2_4	46.7_6	0.077
70[c]	62.9_0	60.9_8	0.072	56.3_9	47.6_4	0.071
80	51.1_3	49.0_8	0.076	...	...	...
80[b]	52.3_2	50.5_1	0.068	45.1_0	34.9_0	0.083
100	20.3	18.3	0.073	12.9	2.4_3	0.085

[a]Usual heat treatment—1 h, 1050 °C, brine quench.
[b]Reannealed 8 h, 1350 °C, brine quench.
[c]New sample, heat treated as above.

cross-sectional area was micrometer limited to ± 0.2%.

C. Measuring procedure

Resistance was measured by passing a constant 1 A through the circuit and comparing the voltage drop across an accurately known length of the specimen with that across a standard resistor. The usual current-reversal procedure for eliminating thermal emf's was employed. Potential contact was made with the specimen by carefully lowering a mutually rigid pair of tungsten needle points onto one of the faces, the specimen being free to see-saw about a central support. The distance between the contacts (about 1.8 cm) was measured with a travelling microscope to an accuracy of ± 0.01%. The probe could be moved along the specimen center line at will, giving reproducible results.

The accuracies of the electrical components used were more than adequate. As a result, the cumulative experimental error, dominated by the uncertainty in cross-sectional area determination, was ± 0.2%.

Resistivities were measured at accurately determined temperatures (a) in air at room temperature, (b) in an ice-chilled alcohol bath, (c) in a dry-ice-chilled alcohol bath, and (d) in liquid nitrogen. From (a) and (b), a $(d\rho/dT)|_{273}^{300}$ was obtained, and the measured resistivities were corrected to 300.0 and 273.2 K, respectively. From (c) and (d) we derived a $(d\rho/dT)|_{77}^{200}$, and corrected the alcohol-bath resistivity to 200.0 K.

III. EXPERIMENTAL RESULTS

A. Pure titantium

The measured resistivities and resistivity temperature dependences of six samples of unalloyed Ti are presented in Table I. The results of the present work are in satisfactory agreement with those of Ames and McQuillan,[10] Hake *et al.*,[11] and Wasilewski.[12] According to the latter author, for example, $\rho_{300} = 47.8$ $\mu\Omega$ cm/K.

Samples 1 through 4 (Table I), prepared from an arc-melted button of TMC Ti[8] were probably less

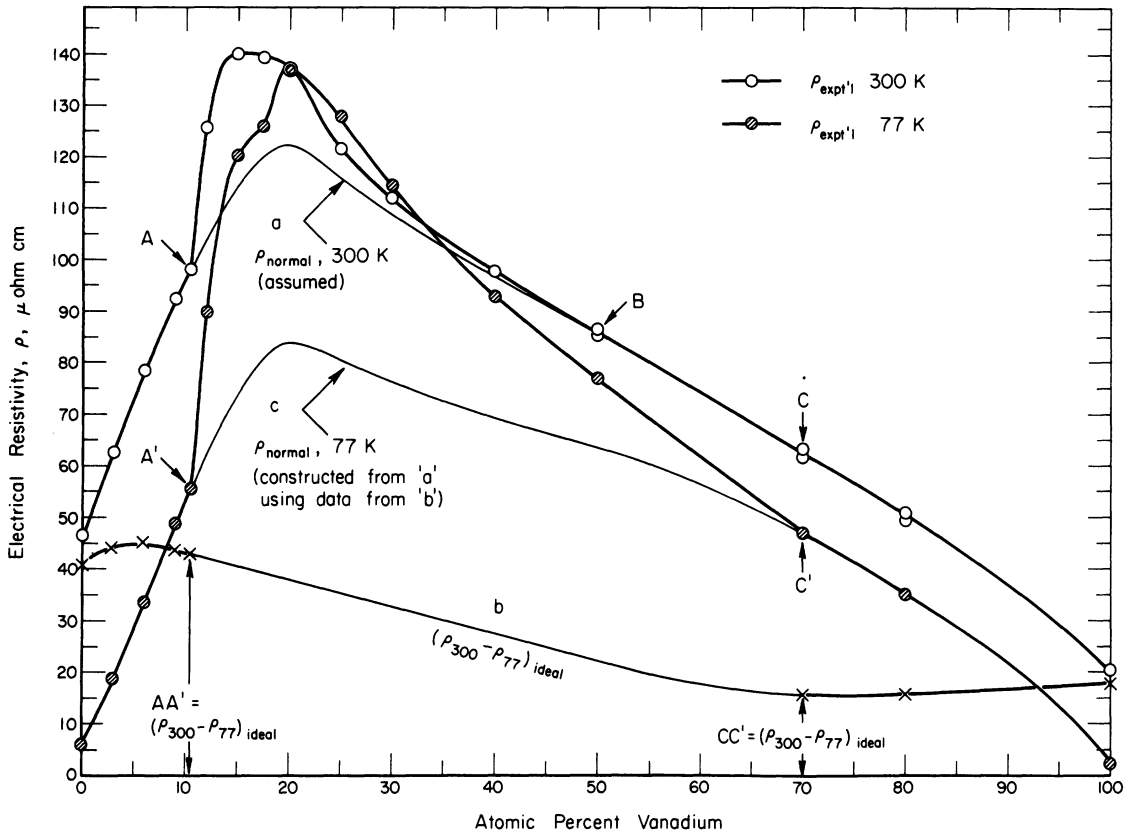

FIG. 5. Graphical analyses of the electrical resistivity data. Reasonable assumptions for (a) $\rho_{normal,300}$ and (b) $(\rho_{300}-\rho_{77})_{ideal}$ are combined in order to estimate a composition-dependence for (c) $\rho_{normal,77}$.

textured and consequently more nearly isotropic in their properties than sample 5 (from swaged rod) and sample 6 (from iodide crystal bar Ti). Accordingly, only the results for the first four samples were included in the final averages reported in Table II. The experimental error of $\pm 0.2_5\%$ in the room-temperature resistivity has been accounted for in the previous section.

B. Ti-V alloys

The measured resistivities and resistivity temperature dependences of 19 samples of Ti-V (3–80 at.%) are listed in Table III. The resistivities at 300, 200, and 77 K are plotted in Fig. 3; and the resistivity temperature dependences of the alloy series, averaged over the ranges 273–300 K and 77–200 K, respectively, are represented in Fig. 4. It is useful to discuss these results with reference to the observed, and deduced, microstructures of the quenched alloys as described in the Introduction. Quenched alloys of up to and including 10.5-at.% V are all completely martensitic (hexagonal-structured α') and their resistivities appear to behave quite normally in their composition dependences and temperature dependences. The same can apparently be said of the essentially bcc V-rich end of the series. However, between 10- and at least 60-at.% V, the alloy resistivity appears to be anomalous with regard to both *composition dependence* (Fig. 3) and *temperature dependence* (Fig. 4).

Referring to Fig. 3, as the solute concentration increases, the occurrence of ω phase in the quenched alloys (from about 12-at.% V) is accompanied by a sharp increase in the resistivity. The maximum in the 300 K resistivity isothermal occurs at about 15-at.% V. This composition, according to Hickman,[13] should be nearly optimal for the occurrence of ω-phase precipitation. At higher V concentrations, the anomalous resistivity component decreases as the precipitate density decreases, or as the precipitation changes character in some other way to be discussed later.

Referring to the resistivity *temperature dependence*, this appears to be anomalously small outside of the α' structural regime, and is actually negative within a composition range centered on 25-at.% V.

TABLE IV. Electron diffraction and lattice-dynamical approaches to ω-phase formation in group-IV-base transition-metal-binary alloys. The headings of the last two columns indicate, in order: technique, author, class of alloy, and approach.

Typical solute concentration ranges in Ti-V	Diffraction effects as seen in electron microscopic studies of quenched alloys[a]	Electron microscopy S. L. Sass[a] Real alloy Static[c]	Lattice-dynamical calculations D. deFontaine[b] Virtual crystal Dynamical[c]
13-at.% V	Sharp ω reflections and straight lines of intensity.	Clusters of rows of particles plus individual rows.	Propagating (long-range) $\frac{2}{3}\langle 1,1,1\rangle$ longitudinal mode of wavelength $(\sqrt{3}/2)$ times (bcc lattice parameter).
13-, 15-, and 19-at.% V	Broad ω reflections and straight lines of intensity.	Rows of 20-Å particles; spaced 22 Å; typically 5 to a row.	$\frac{2}{3}\langle 1,1,1\rangle$ vibrational modes tending to become more localized and less coherent.
25-at.% V	Broad ω reflections, lines of intensity curved.	Isolated 15-Å particles.	
25-55 at.% V	Weak, broad lines of intensity, becoming diffuse and circular as solute concentration increases.	Not interpretable in terms of of precipitation.	Curvilinear diffuse reflections due to pronounced coupling between local vibrational modes.

[a]Reference 19.
[b]Reference 18.
[c]These two columns are coupled by the following: (1) the dynamical effect yields a static (observable) atomic displacement through anharmonicity; (2) the ω phase becomes "frozen in" as a result of solute-solvent interdiffusion in a real alloy.

IV. GRAPHICAL ANALYSIS OF THE Ti-V RESISTIVITY DATA-EXTRACTION OF AN ANOMALOUS RESISTIVITY COMPONENT

In experimental studies of departures from Matthiessen's rule, or other deviations from a simple additivity relationship for resistivity, it has always been difficult to know what to subtract away from the measured resistivity in order to arrive at a "true" anomalous component, ρ_{anom}. In this section we start with a reasonable assumption regarding the composition dependence of ρ_{anom} at 300 K, in order to say something about the temperature dependence and composition dependence of ρ_{anom} between room temperature and 77 K.

A. Initial assumptions

(i) According to Sass,[5] measurable ω-phase-related electron-diffraction effects were observable at room temperature in quenched Ti-V alloys of solute concentrations as high as 45–55-at.% V. Accordingly, in Fig. 5 we draw a smooth curve *a* between the onset *A* of ω-phase precipitation and *B*, a point of inflection in the resistivity curve, in such a way that the anomalous resistivity follows the expected density of ω-phase precipitation as depicted in Fig. 6(a). That is, $\rho_{\text{anom, 300}}$ is made to increase monotonically (with decreasing [V]) to a maximum at 14-at.% V, the near-optimal composition for the precipitation [Fig. 6(b), 300-K curve].

(ii) The second assumption is that normal-resistivity temperature dependence exists only in the regions in which the 300 and 77-K isothermals are "parallel," i.e. below AA' and above CC'; and that between these limits the *ideal* temperature dependence varies smoothly with composition (in fact, linearly over most of the range) as indicated by the line segment *b* in Fig. 5.

B. Graphical analysis

With the above assumptions, it is possible to construct curve *c* to represent "normal" alloy resistivity at 77 K. Based on that curve, a $\rho_{\text{anom},77} = (\rho_{\text{expt}} - \rho_{\text{normal}})_{77\text{ K}}$ was obtained and plotted along with $\rho_{\text{anom},300}$ in Fig. 6(b).

Curve *a* of Fig. 6(c) represents the amount by which ρ_{anom} *increases* as the temperature decreases from 300 to 77 K; curve *b* represents ρ_{ideal}, a competitive *decrease* in resistivity with decreasing temperature. In the concentration range in which $(\rho_{300} - \rho_{77})_{\text{anom}}$ is dominant (viz. 20–33-at.% V) the temperature coefficient of total alloy resistivity, in the liquid-nitrogen range, is negative. It is reassuring to note that this result of the graphical analysis turned out to be in complete agreement with the composition range of experimentally ob-

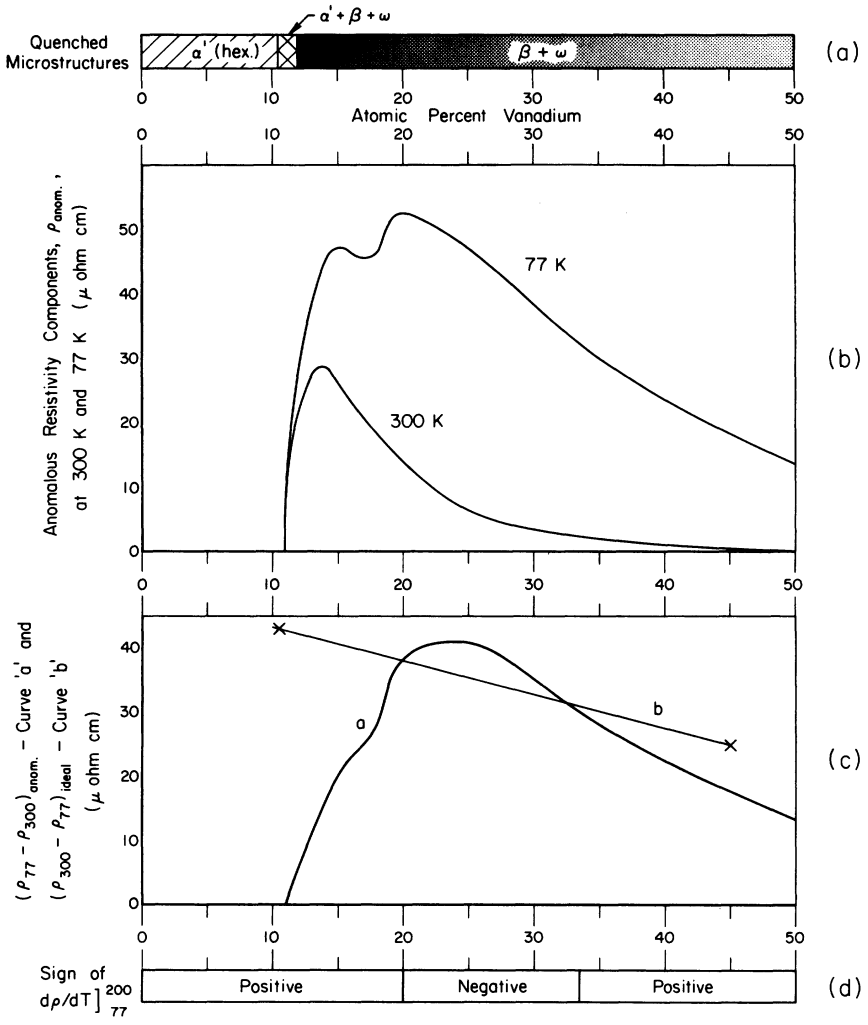

FIG. 6. (a) Indication of the composition ranges of ice-brine-quenched microstructures. (b) Anomalous resistivity components at 300 and 77 K respectively, deduced from Fig. 8 by taking the differences ($\rho_{expt} - \rho_{normal}$) at the two temperatures. (c) The competing temperature-dependent resistivity components—$\rho_{anom.}$ (curve *a*; $d\rho/dT$ negative) and ρ_{ideal} (curve *b*; $d\rho/dT$ positive). (d) Diagram indicating the range over which, according to the graphical analysis, the net $d\rho/dT$ is negative. The range of negative temperature dependence so obtained is consistent with the direct experimental results, cf. Fig. 5.

served negative temperature coefficients; cf. the $(d\rho/dT)|_{77}^{200}$ curve in Fig. 4.

C. Mean free path for anomalous scattering

Following Hake's study of some electronic and superconductive properties of various type-II superconductors,[14] we employ the following formula for the electronic mean free path Λ:

$$\Lambda = 1.27\times10^{4}[\rho_n n^{2/3}(S/S_f)]^{-1} \text{ cm} , \quad (1)$$

where ρ_n is the alloy resistivity in Ω cm, n is the number of conduction electrons per cm^3, and S/S_f is the ratio of the Fermi-surface area to that of a free-electron gas of density n.

Hake[14] has suggested that $S/S_f = 0.6$, and gives a value for n of 2.58×10^{23} electrons/cm^3 for Ti-V (25 at.%). We assume these values to be constants in the composition range of interest to us here (which is centered about 25-at.% V) and calculate Λ from the resistivity expressed in $\mu\Omega$ cm, using the relationship

$$\Lambda = 516/\rho \text{ Å} . \quad (2)$$

A mean free path model for alloy resistivity assumes that

$$\rho = \rho_{normal} + \rho_{anom} = \text{const}\,(\Lambda_{normal}^{-1} + \Lambda_{anom}^{-1}) . \quad (3)$$

In this approximation we apply Eq. (2) to the anomalous resistivity data of Fig. 6(b) to derive mean free paths for anomalous scattering at 77 and 300 K. These results are plotted in Fig. 7. At room temperature, the precipitate scattering in a 14-at.% V alloy can be represented by a mean free path of 18 Å; while at 77 K, additional scattering of some kind, represented by a mean free path of 10–11 Å, appears reversibly, with respect to temperature, over a wide concentration range.

According to the work of Sass,[5] ω-phase precipitation in quenched Ti-V (13 – 15 at.%) alloys takes the form of distinct rows, or clusters of rows, of particles 10 – 20 Å in size, spaced some 22 Å apart. This result would not be inconsistent

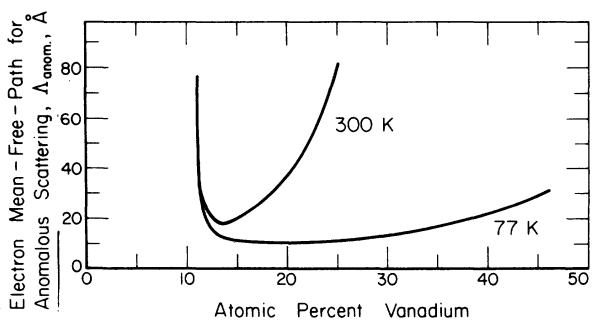

FIG. 7. Mean free path Λ(Å) for anomalous scattering at 300 and 77 K, calculated from the anomalous resistivity components ρ_{anom} ($\mu\Omega$ cm), using $\Lambda = 516/\rho$.

with the 18-Å mean free path for anomalous scattering at room temperature deduced for alloys of compositions near 14-at.% V. We suggest, however, that the *reversible* anomalous scattering, which seems to be present in alloys at least as far out as 70-at.% V, is associated not with precipitate particles themselves, but with the bcc lattice instability which gives rise to them under suitable conditions.

V. DISCUSSION OF THE RESULTS

A. ω-phase and related structural anomalies in Ti-V alloys

The precipitation of ω phase in Ti- and Zr-base transition-metal binary alloys has been discussed by Hickman,[13] and reviewed by Hickman[15] and Sass.[16] The bcc→ω transformation and the crystallography of ω phase have been considered in detail by Sass and his students[17]; and the lattice dynamics of the transformation have been studied by de Fontaine and coworkers.[18] The results of these investigations, to be outlined briefly here, have direct bearing on (a) the anomalous-resistivity *composition dependence;* (b) the anomalous *temperature dependence* (of which the *negative* temperature dependence is an extreme case); and (c) phase stability in transition-metal binary alloys, and its relationship to their superconductivity.

Table IV summarizes and compares the electron microscopic (Sass[17]) and lattice dynamical (de Fontaine[18]) approaches to ω-phase precipitation in Ti-V-like alloys. The two points of view presented are entirely compatible to the extent that a real alloy, after quenching from an elevated-temperature anneal, can be represented by a virtual crystal (in which the two atomic species of the binary alloy share common average properties). Departures from a purely lattice-dynamical approach must occur in a real alloy when diffusion intervenes, as it usually does to some extent, even during the quenching process itself. Consequently, it is useful to treat a real, quenched alloy using a combination of both models, with reversible ω-phase-type behavior being described in terms of phonons, and with irreversible properties being regarded as the result of diffusion-fixed precipitate particles.

The picture represented by Table IV is as follows. At high solute concentrations, bcc instability manifests itself as coupled local vibrational modes (virtual phonons). Electron-diffraction effects are observable, but there is no evidence of precipitation of any kind. As the solute concentration decreases, there is an accompanying continuous change in the lattice dynamics. In particular, the vibrational states become less localized and more nearly states of the crystal. In conjunction with vibrational anharmonicity, this leads to average displacements of certain atomic planes within small regions of the crystal (i.e. "structural precipitates"). If the time-temperature product is suitable, the precipitates can be irreversibly fixed by solute-solvent interdiffusion. In sufficiently dilute alloys (e.g., ~14–15-at.% V in Ti-V), copious phonon-induced structural transformation to ω phase takes place without diffusion, since the ω phase which forms will already be at its equilibrium composition. In practice, however, near this end of the composition spectrum, the hexagonal phase is so highly favored that an appreciable fraction of the material tends to transform all the way to the hexagonal α' rather than to ω phase.

The existence of the longitudinal phonons of wave vector $\vec{q} = \frac{2}{3}\langle 1, 1, 1\rangle$ (Table IV) is an expression of bcc instability. The structural result of the existence of such modes (i.e., the accompanying "displacement wave"[18]) is referred to as "athermal" ω phase, while the presence of solute-solvent interdiffusion leads in turn to the establishment of so-called "isothermal ω phase," irreversible under thermal cycling in the temperature range below room temperature.

B. Precipitate-induced anomalous resistivity

According to Sass,[17] precipitate particles have been seen at room temperature in Ti-V alloys of compositions out to 25-at.% V. Although temperature-dependence studies of precipitation of this kind have not been recorded, it is most likely that the dark-field-observable precipitation is diffusion controlled or irreversible in the above sense. de Fontaine *et al.*,[18] in diffraction studies, have noted diffusionless (and consequently reversible or "athermal") ω phase in Ti-V (19 at.%). It is therefore likely that both permanent precipitates *and* phonon-induced anomalies coexist out to 25-at.% V. We suggest that a significant fraction of the anomalous resistivity noted in the room-temperature-

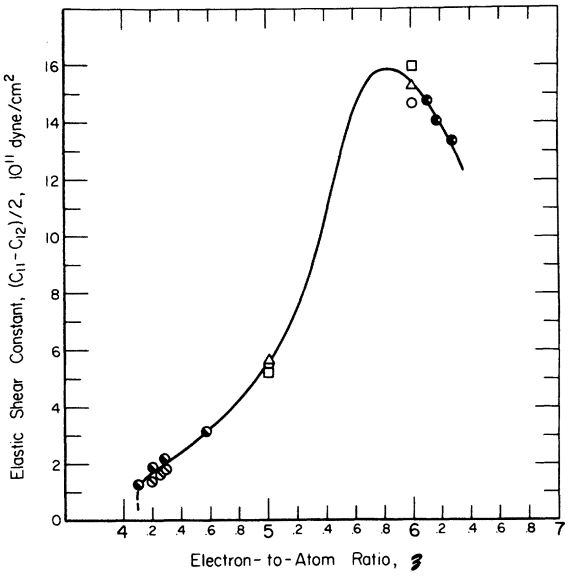

FIG. 8. Elastic shear modulus $C' = (c_{11} - c_{12})/2$ for various transition metals and binary alloys. The curve suggests that the bcc phase has maximal stability for $\mathfrak{z} \sim 5.9$. Symbols O refer to V (Ref. 24) and Cr (Ref. 25); the Δ refer to Nb (Ref. 24) and Mo (Ref. 26); the □ refer to Ta (Ref. 27) and W (Ref. 27). The alloy systems represented on the extreme left are Ti-Cr (Ref. 28) and Zr-Nb (Ref. 19), symbolized by ◐ and ◑ respectively, while that on the extreme right is Mo-Re (Ref. 26), ●.

resistivity composition dependence is a result of permanent ω-phase precipitation.

C. Phonon-induced anomalous resistivity

As discussed in Sec. VA above, with reference to Table IV, ω-phase precipitation in sufficiently dilute Ti-V-type alloys may be regarded as either particulate, or a result of coherent atomic displacements. If conditions are such that solute-solvent interdiffusion does not take place (i.e., either the alloy composition is equal to the saturated or equilibrium ω-phase composition, or the quench rate is ultrarapid), a description of either incipient or actual ω phase in terms of phonons is more useful. The implications of such a description are discussed in this section.

In a given alloy, the density of "ω-phonon" states is reversibly and inversely related to the temperature. Isothermally, the density of states (and the phonon lifetimes—Table III) decreases as the solute concentration increases; and the modes become more localized. According to Sass[17] and de Fontaine,[18] the unstable bcc lattice supports a longitudinal acoustic wave of wavelength $(\sqrt{3}/2)$ times the lattice parameter. Such short-wavelength nonthermally activated modes, or soft phonons, make strong contributions to electrical resistivity. At low temperatures the effect of such modes will dominate other forms of scattering except perhaps umklapp processes which, when they occur, are also capable of producing large electron momentum changes. We suggest that the reversible anomalous resistivity is a result of scattering by instability-related soft phonons.

Figure 6(b) shows that, although for Ti-V alloys in the composition range 20–34-at.% V the reversible anomalous resistivity dominates the ideal component leading to a net negative $d\rho/dT$, the 77-K anomalous component itself exists to a significant extent in alloys of compositions well beyond 50-at.% V (cf. Table III—diffraction effects, 25–55-at.% V). Indeed, on the basis of the anomalous electron-diffraction effects reported by Sass[19] for both pure Nb and V, it is likely that a resistivity component due to scattering by local soft phonons exists to some extent in all three pure-group-V transition elements at room temperature.

D. Phase stability and superconductivity in bcc transition metals and alloys

Up to this point, we have been considering the experimentally observed anomalous resistivity in Ti-V, and its origin in terms of bcc-lattice-instability-related soft-phonon scattering. But since Ti-V and similar alloys such as Zr-Nb and Ti-Nb (i.e., IV-V transition-metal alloys) are type-II superconductors with "high" (for alloys) transition temperatures, it is inevitable that a connection should be made between their anomalous normal-state resistivity and some of their superconductive properties.

Group-IV transition elements are hcp at ordinary temperatures while the group-V metals are bcc. Accordingly, we would expect a decrease in bcc stability upon alloying a group-V element with one to the left of it in the Periodic Table. A measure of relative bcc lattice stability is the elastic shear modulus $C' = \frac{1}{2}(c_{11} - c_{12})$, since this indicates the ease with which a cubic → hexagonal shear can take place. Figure 8 relates C' to $\mathfrak{z}$ for the bcc transition metals V, Nb, and Ta (group V); Cr, Mo, and W (group VI); and some binary alloys. It suggests that the bcc lattice has greatest stability, by the C' criterion, for $\mathfrak{z} \simeq 6$; and that the stability decreases rapidly toward $\mathfrak{z} = 4.1$. According to Fig. 8, the lattices of group-V elements, although bcc, are of "limited stability," in agreement with the electron-diffraction results referred to above. The alloying of group-V elements to the left produces further decrease in bcc stability, which manifests itself first as localized or incoherent phonons, and eventually to the propagating short-wave phonons which yield the ω-phase phenomenon. We suggest that the soft phonons which characterize the bcc instability favor phonon-moderated elec-

tron-electron coupling and hence superconductivity, as long as the lattice is essentially bcc. This is an example (cf. Fröhlich[20]) of a high normal-state resistivity's being consistent with superconductivity at sufficiently low temperatures. But these same phonons lead to the formation of ω phase, which itself has a very low transition temperature, comparable to that of pure hcp Ti.[21] Although a two-phase $\beta+\omega$ alloy undergoes a *bulk* superconducting transition,[21,22] its transition temperature is some proximity-effect controlled weighted average.[23] In a previous paper[1] dealing with superconductivity in Ti-Mo, we have argued that if ω-phase precipitation could somehow be inhibited as $\vec{s}$ decreased into the unstable β regime, T_c would increase monotonically. As $\vec{s}$ decreases in a series of real alloys, superconductivity in the unstable bcc phase competes with the tendency for the hexagonal-structured product of the instability to remain normal. Thus in IV-V transition-metal binary alloys, the T_c-vs-$\vec{s}$ curves always possess maxima.

VI. SUMMARY

The results of electrical resistivity (ρ) measurements on Ti-V alloys exhibit both anomalous composition dependences ($d\rho/dc$) and anomalous temperature dependences ($d\rho/dT$). It has been argued that these anomalies arise through electron scattering by large-$\vec{q}$ phonons, the existence of which is an expression of bcc lattice instability. This instability, already present to some extent in pure V, increases as the solute concentration decreases down to the threshold of martensitic transformation (10.5–12-at.% V). The average atomic displacements which accompany the soft phonons of the instability yield ω phase at sufficiently low concentrations, or precursor effects at higher concentrations. These same phonons, which result in a high normal-state resistivity, also favor superconductive coupling and consequently a relatively "high" T_c. On the other hand, this effect must compete with a proximity-effect-induced lowering of T_c by the product (ω phase) of the lattice instability.

ACKNOWLEDGMENT

Technical assistance by C. J. Martin (electron microscopy) and R. D. Smith (heat treatment and optical metallography) is gratefully acknowledged.

---

*Supported by the Air Force Office of Scientific Research (AFSC) under Grant No. 71-2084.

[1]E. W. Collings, J. C. Ho, and R. I. Jaffee, Phys. Rev. B 5, 4435 (1972).

[2]J. C. Ho and E. W. Collings, Phys. Rev. B 6, 3727 (1972).

[3]E. W. Collings and H. L. Gegel, Scr. Metall. 7, 437 (1973).

[4]K. K. McCabe, MS thesis, (Cornell University, Ithaca, New York, 1970) (unpublished). See also K. K. McCabe and S. L. Sass, Philos. Mag. 23, 957 (1971).

[5]ω-phase precipitation in Ti-Mo is considered in Refs. 1 and 2. For an excellent review of the occurrence and composition of ω phase in various alloys, Ref. 4, pp. 2–7 is strongly recommended.

[6]H. K. Adenstedt, J. R. Pequignot, and J. M. Raymer, Trans. Am. Soc. Met. 44, 990 (1952).

[7]F. R. Brotzen, E. L. Harmon, and A. R. Troiano, Trans. AIME, J. Metals, 203, 413 (1955).

[8]The electrorefined titanium sponge (>99.8%), grade *ELXX*, from the Titanium Metals Corp. (TMC), contained as principal impurities in ppm by weight—Cl, 590; O, 410; Na, 220; Sn, <200; C, 100; Cr, 60. The vanadium (99.95%), VP grade, from Materials Research Corp. (MRC), contained as principal impurities in ppm by weight—O, 200; Cr, 100; Fe, 100; N, 20.

[9]The less severe heat treatment had been selected in the first instance, as a precaution against oxygen contamination of the specimens.

[10]S. L. Ames and A. D. McQuillan, Acta Metall., 2, 831 (1954).

[11]R. R. Hake, D. H. Leslie, and T. G. Berlincourt, J. Phys. Chem. Solids 20, 177 (1961).

[12]R. J. Wasilewski, Trans. Metall. Soc. AIME 224, 5 (1962).

[13]B. S. Hickman, J. Inst. Met. 96, 330 (1968); Trans. Metall. Soc. AIME 245, 1329 (1969). During aging of a ($\beta+\omega$) Ti-V alloy, diffusion takes place until the ω contains 13.5–14-at.% V. It follows that "athermal" ω phase (i.e., that which occurs in the absence of diffusion) should occur most abundantly in Ti-V (~14 at.%).

[14]R. R. Hake, Phys. Rev. 158, 356 (1967).

[15]B. S. Hickman, J. Mater. Sci. 4, 554 (1969).

[16]S. L. Sass, J. Less-Common Met. 28, 157 (1972).

[17]Reference 4—Ti-V. See also S. L. Sass, Acta Met. 17, 813 (1969)—Zr-Ti; C. W. Dawson and S. L. Sass, Met. Trans. 1, 2225 (1970)—Zr-Nb; and A. T. Balcevzak and S. L. Sass, Met. Trans. 3, 1601 (1972)—Ti-Nb.

[18]D. de Fontaine, Acta Met. 18, 275 (1970); D. de Fontaine, N. E. Paton, and J. C. Williams, Acta Met. 19, 1153 (1971).

[19]S. L. Sass, J. Less-Common Met. 28, 157 (1972)—Nb; S. L. Sass (private communication)—V.

[20]H. Fröhlich, Phys. Rev. 79, 845 (1950).

[21]J. C. Ho and E. W. Collings, in *Titanium Science and Technology*, edited by R. I. Jaffee and H. M. Burte (Plenum, New York, 1973), pp. 815–830.

[22]J. C. Ho and E. W. Collings, Phys. Lett. A 29, 206 (1969).

[23]E. W. Collings and J. C. Ho (unpublished).

[24]D. I. Bolef, J. Appl. Phys. 32, 100 (1961).

[25]D. I. Bolef and J. de Klerk, Phys. Rev. 129, 1063 (1963).

[26]D. L. Davidson and F. R. Brotzen, J. Appl. Phys. 39, 5768 (1968).

[27]F. H. Featherston and J. R. Neighbours, Phys. Rev. 130, 1324 (1963).

[28]E. S. Fisher and D. Dever, Acta Met. 18, 265 (1970).

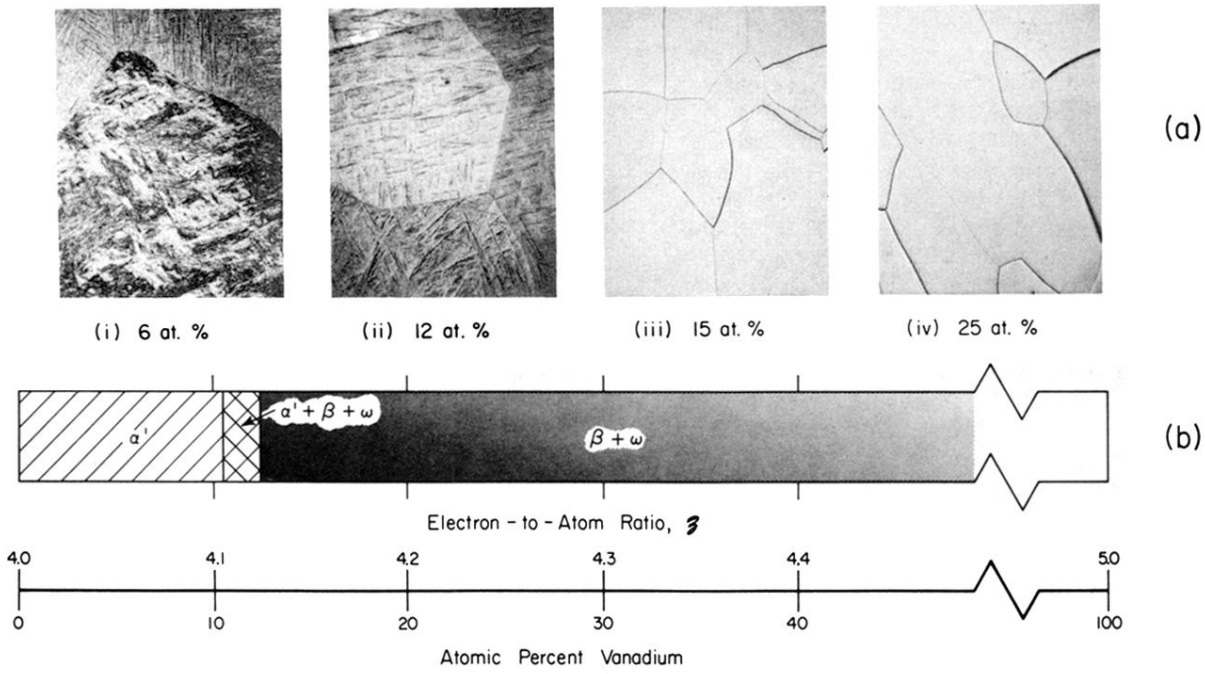

FIG. 2. (a) Optical micrographs (original magnification 50×) of representative quenched Ti-V alloys. (b) Structure observed, or deduced to be present, in 30-g ingots after quenching into iced brine.

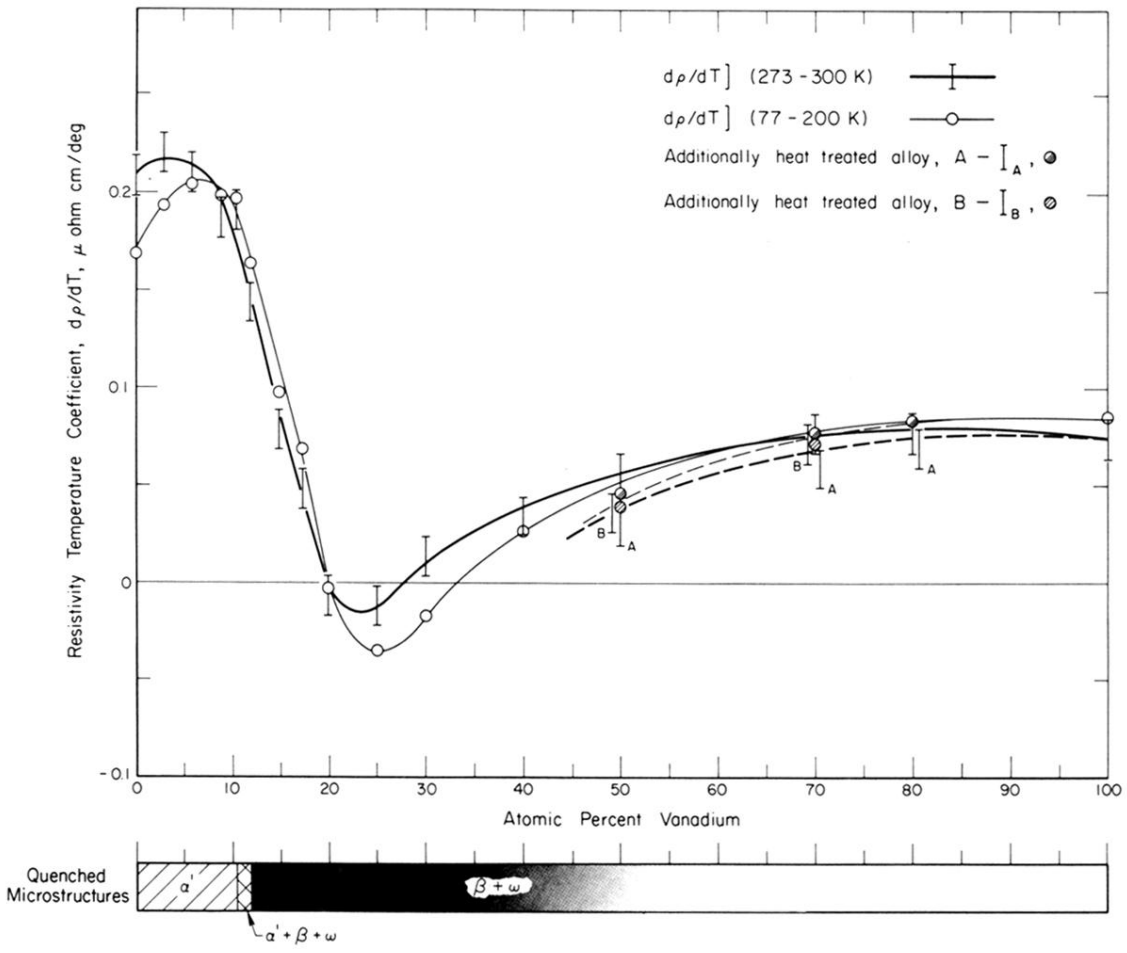

FIG. 4. Resistivity-temperature coefficients in two temperature ranges (273–300 K and 77–200 K) for Ti-V alloys. Additional heat treatment produced slight changes in the submicrostructures, resulting in small changes in resistivity-temperature dependences as indicated by the chain lines.